6-19-2018

Young Blue Straggler Stars in the Galactic Field

Gemunu Ekanayake
Manhattanville College

Ronald Wilhelm
University of Kentucky, ron.wilhelm@uky.edu

Young Blue Straggler Stars in the Galactic Field

Monthly Notices
of the
ROYAL ASTRONOMICAL SOCIETY

MNRAS **479,** 2623–2629 (2018)
Advance Access publication 2018 June 19

doi:10.1093/mnras/sty1621

Young blue straggler stars in the Galactic field

Gemunu Ekanayake[1]★ and Ronald Wilhelm[2]

[1]*Department of Physics, Manhattanville college, Purchase, NY 10577, USA*
[2]*Department of Physics and Astronomy, University of Kentucky, Lexington, KY 40506, USA*

Accepted 2018 June 15. Received 2018 June 11; in original form 2018 May 22

ABSTRACT

In this study, we present an analysis of a sample of field blue straggler (BS) stars that show high ultra violet emission in their spectral energy distributions (SEDs): indication of a hot white dwarf (WD) companion to BS. Using photometry available in the Sloan Digital Sky Survey (SDSS) and Galaxy Evolution Explorer (GALEX) surveys, we identified 80 stars with ultraviolet (UV) excess. To determine the parameter distributions (mass, temperature, and age) of the WD companions, we developed a fitting routine that could fit binary model SEDs to the observed SED. Results from this fit indicate the need for a hot WD companion to provide the excess UV flux. The WD mass distribution peaks at $\sim$0.4 $M_{\odot}$, suggesting the primary formation channel of field BSs is case B mass transfer, i.e. when the donor star is in red giant phase of its evolution. Based on stellar evolutionary models, we estimate the lower limit of the binary mass transfer efficiency to be $\beta \sim 0.5$.

Key words: blue stragglers – white dwarfs – binary stars – SDSS – GALEX.

1 INTRODUCTION

Blue straggler stars were first discovered in a photometric study of globular cluster M3 by Sandage in 1953 (Sandage 1953). They are identified by their position in color magnitude diagram, in which they appear along the extension of the main sequence but bluer and brighter than the main sequence turn-off, giving the appearance of a younger stellar population. The BS sequence is a typical feature of most globular clusters. Since Sandage's discovery, blue stragglers have been observed in many stellar environments, including open star clusters (Mathieu & Geller 2009), globular clusters (Ferraro et al. 1999), dwarf spheroidal galaxies (Momany et al. 2007), and the Galactic field (Preston & Sneden 2000).

The exact mechanism for the formation of blue stragglers is still not fully understood. Single star evolutionary theory fails to explain the existence of BS stars since it is not possible for stars to have masses greater than the main-sequence turn-off in a single epoch star formation environment. Under the correct circumstances, however, it is possible for stars to gain significant mass long after the star formation epoch has ended. Two leading theories rely on the basic idea that BSs are formed by adding mass to a main sequence star in a binary or multiple stellar system via some interaction mechanism. (1) Mass transfer between two stars in a binary system: This is the case where the more massive star in a binary system transfers material, during its post main-sequence phase, to its companion star. Though still not fully understood, McCrea (1964) provided the first, seminal idea of mass transfer and its consequences during binary evolution. If the mass transfer is stable, this may add sufficient mass to the secondary to convert it into a blue straggler. This appears to be the main formation channel for BS stars, particularly in the low-density environment of the Galactic field. Convincing evidence for operation of this process was reported by Gosnell et al. (2014) for three stars in the old open cluster NGC 188. (2) Merger between stellar systems: This could happen in various scenarios, such as the merger of a contact binary, a merger during a dynamical encounter and a merger of an inner binary in hierarchical triple system. In such a scenario, it is expected that the merged stars will form a single more massive star.

Generally the mass transfer binaries are classified on the basis of the evolutionary phase of the donor (Kippenhahn & Weigert 1967). Case A: Mass transfer occurs during hydrogen core burning phase of the donor. This can happen if the orbital separation of the binary is small (usually an orbital period of a few days). Case B: Mass transfer occurs after exhaustion of hydrogen in the core of the donor and the donor enters the red giant phase. In this case, orbital period is about 100 days or less, but significantly longer than case A. Case C: Mass transfer occurs after exhaustion of core helium (He) burning and the donor enters the AGB phase. Here the orbital period is generally greater than 100 d. It is believed that case A mass transfer is more likely to be result in the coalescence of the two stars (Chen & Han 2009). In that sense it can be treated as one of the merger scenarios. According to the binary evolution simulations (Chen & Han 2009), in order to produce a BS via case B or case C, the mass transfer has to be stable. During stable mass transfer, the donor stays within its Roche-lobe. Therefore, the stability of the mass transfer depends on the donor's response to the mass loss, on how conservative the process is, and on the angular momentum

★ E-mail: gbe8396@gmail.com

loss processes in this binary. Given stable mass transfer, case B will result in a He white dwarf companion bound to the blue straggler, while in case C the remnant companion is a CO white dwarf.

1.1 Field blue straggler stars

For a given stellar population, the dominant formation channel of BSs depends on its environment. The BSs in the Galactic field, where the stellar number density is much lower than globular clusters, are formed primarily from binary mass transfer (Preston & Sneden 2000). High-resolution study of Field BSs done by Preston and Sneden (Preston & Sneden 2000) suggested that 60 per cent of their sample consisted of binaries. Moreover, they concluded that the great majority of field BSs are probably created by Roche-lobe overflow during red giant branch evolution (case B). Ryan et al. (2002) studied lithium deficiency and rotation of the BSs and came to the conclusion that these stars can be regarded as mass transfer binaries.The origin of BSs in the Galactic field is clearly tied to the overall formation of the Galactic halo. Since star formation ended in the halo over 10 giga-years ago, most identified BSs originate through case B/C evolution. The exception, as argued by Preston & Landolt (1999), is a modest fraction of BSs that may actually be young, massive stars that have been accreted from Galactic satellites that contain young stellar populations.

To test the theory with observations, it is vital to identify the clean sample of mass transfer candidates. Because blue stragglers in globular clusters are contaminated by those formed via collisions, field blue stragglers are the best candidates for a clean sample of mass-transfer BSs. As mentioned above, the mass-transfer process results in a BS with a white dwarf companion. BSs are much brighter than WDs at optical wavelengths so, such binaries are difficult to observe directly. However, if the WD companions to BS are sufficiently young and hot, they can be detected at ultraviolet (UV) wavelengths. Studying a sample of such recent BS/WD systems can set constraints on the mass transfer formation mechanism. In this paper we present a study of field BSs that show UV excess in their SED, in order to characterize their mass transfer history. Sections 2 and 3 describe the methodology for identifying the UV excess stars by the use of the SDSS and GALEX photometry. Section 4 summarizes our analysis and techniques used to determine the WD parameters. A brief discussion and our conclusions are provided in Section 5.

2 DATA

Over the years many photometric studies have been done to identify field BSs, primarily using color–color plots. For example, Yanny et al. (2000) identified 2700 field BSs using SDSS photometry. Sirko et al. (2004) used SDSS photometry in combination with spectroscopy to identify field BSs.

The data used for this study were taken from the Sloan Digital Sky Survey Data Release 12 (SDSS DR12) and Galaxy Evolution Explorer (GALEX) GR5, an UV survey.

2.1 SDSS Data

SDSS DR12 offers the latest data from SDSS project 3. It provides photometry in five bands (u, g, r, i, and z) for 400 million objects and low-resolution spectroscopy with resolution $R \sim 1800$ and wavelength coverage 3800-9200 Å, for about two million objects.

Field BSs can be identified in a $u - g$ versus $g - r$ diagram by the use of the following color cuts.

$$0.60 < (u - g) < 1.60 \quad (1)$$

$$-0.20 < (g - r) < 0.05 \quad (2)$$

This area in the color–color diagram is populated by A-type stars, including high-gravity BS and low-gravity BHB stars. Therefore, in order to separate the BSs from BHB stars, one would need stellar parameters for individual stars. For that purpose we employed the current version of the Sloan Extension for Galactic Understanding and Exploration (SEGUE) Stellar Parameter Pipeline (SSPP) (Lee et al. 2008). We select only the BSs above 7000 K to avoid contamination of other F,G-type main sequence stars and/or variable RR lyrae stars.

2.2 GALEX Data

GALEX photometry was performed in two UV bands, far-UV (FUV) and near-UV (NUV). The effective wavelengths are 1516 and 2267 Å for FUV and NUV bands, respectively.

2.3 Cross-identification of sources

Most GALEX observations were designed to cover the SDSS footprint at a comparable depth. Constructing spectral energy distributions (SEDs) that range from UV to IR requires combining SDSS sources to GALEX counterparts. The matching was done on line by use of the CDS X-Match Service,[1] adopting a match radius of 5 arcsec. Such a match highly depends on the positional accuracy and resolution of both surveys. Because the GALEX images have lower angular resolution, there are cases with multiple GALEX matches per given SDSS source. These comprise about 10 per cent of our total sample. In such cases we used only the closest distance matches. In vast majority of cases (>90 per cent), GALEX and SDSS sources are matched within 2 arcsec. Our final sample includes 2188 stars.

SDSS data were corrected for interstellar extinction using the extinction relations given in Schlafly & Finkbeiner (2011), while FUV and NUV were corrected for extinction using the relations given in Rey et al. (2007).

3 UV-EXCESS STARS

Identification of UV-excess stars based on their position in FUV/optical color–color plot is one useful application of UV photometry. Using GALEX and SDSS colors together has enabled the discovery of white dwarf-main sequence binary systems, i.e. binaries with WD primaries and late-type main-sequence secondaries (Rebassa-Mansergas et al. 2012)

Smith et al. (2014) adopted a similar approach to identify the FGK-type stars with excess UV in their SED. They used combined data from GALEX satellite's FUV and NUV bandpasses as well as from the ground-based SDSS survey and the Kepler Input Catalog to identify stars that exhibit FUV-excesses relative to their NUV fluxes and spectral types. They considered that these UV excesses originate from various types of hot stars, including white dwarf DA and sdB stars, binaries, and strong chromosphere stars that are young or in active binaries. They calibrate the UV-excess stars using their distribution in (FUV − NUV) − $T_{\rm eff}$ plane (fig. 3 of Smith

[1] http://cdsxmatch.u-strasbg.fr/xmatch

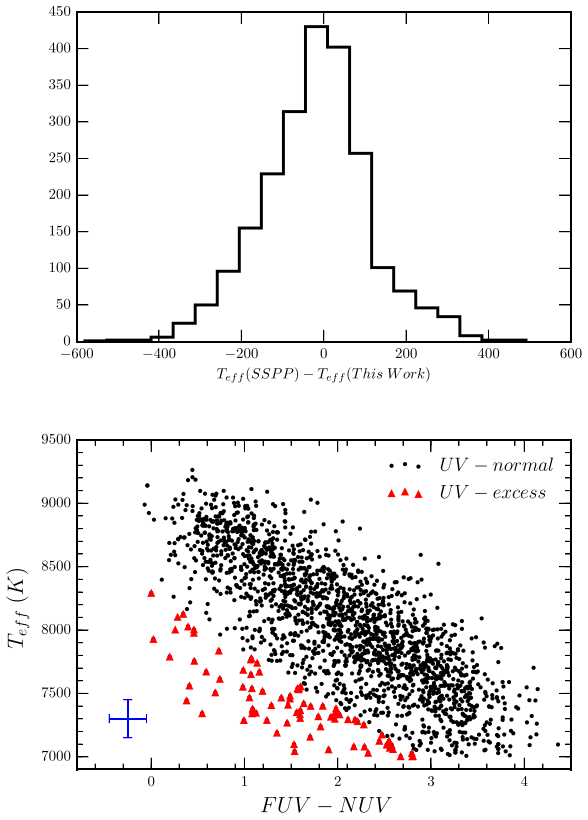

Figure 1. Top: Comparison of temperatures of BSs in this work with SSPP. Bottom: (FUV-NUV) versus SSPP temperature values from SDSS-GALEX data. Data represented by red triangles deviate more than 2σ from the fit to the main diagonal sequence and identified as BSs with UV-excess.

et al. 2014). We adopted a similar method in selecting BS UV-excess stars.

3.1 Temperature sanity check

The method for selecting UV excess BSs depends on the temperatures of the stars. Rather than simply adopting the SSPP $T_{\rm eff}$ values directly, we remeasured the temperatures for our sample stars by fitting the Hydrogen Balmer lines of each SDSS spectrum to model synthetic spectra. A grid of synthetic spectra, spanning the stellar parameter range of our sample, was generated using Kurucz ATLAS12 atmosphere models[2] and the spectral synthesis routine, SPECTRUM (Gray & Corbally 1994). In order to achieve a finer grid resolution, we interpolate the Kurucz models using KMOD IDL package.[3] KMOD interpolates linearly a Kurucz model for the desired values of effective temperature, surface gravity, and metallicity using eight surrounding models. Our final grid consists of spectra with the temperatures in the range 6500–10 000 K in steps of 125 K. Finally the point estimates of mean and error in temperatures were calculated. The mean error obtained for temperatures is 140 K. We compared the temperatures obtained from our method to those obtained from the SSPP in order to check the consistency (Fig. 1a). Both SSPP and our method predicts consistent values for the majority of the stars. We excluded from our sample any stars that have a $T_{\rm eff}$ difference larger than 250 K. Given the larger uncertainties in our measurements, we have adopted the SSPP $T_{\rm eff}$ values for our final sample.

We plotted $T_{\rm eff}$ values determined from the SSPP versus (FUV − NUV) color of the stars in our sample (Fig. 1). The diagonal sequence in Fig. 1 reflects the relationship between SDSS $T_{\rm eff}$ and (FUV − NUV) for the main-sequence stars. We fit the main diagonal sequence with a quadratic fit and we identify stars lying more than 2σ below the regression as UV-excess BS stars. These are our candidates for the BSs with a hot WD companion. Their GALEX and SDSS photometry, along with their stellar parameters, are given in Table A1.

4 BS-WD SED FITTING

In order to obtain the stellar parameters of BS-WD binaries, we fit the observed SEDs of UV-excess stars with a composite model SEDs composed of BSs and white dwarfs. We employed a theoretical grid of spectra (Castelli & Kurucz 2004) with $6000 < T_{\rm eff} < 10\,000$ K in steps of 250 K, $0.5 < \log g < 5.0$ in steps of 0.5, and $-2.5 <$ [Fe/H] < 0.5 in steps of 0.5.

For white dwarf models we employed the theoretical color tables developed by Bergeron (University of Montreal, private communication). For these models, stellar masses and cooling ages are obtained from a detailed evolutionary cooling sequences appropriate for these stars. For the white dwarfs with pure hydrogen model atmospheres above temperatures 30 000K, the carbon-core cooling models of Wood (1995) with thick hydrogen layers of $M_{\rm H}/M* = 10^{-4}$ were used. For temperatures below 30 000K, cooling models similar to those of Fontaine et al. (2001) but with carbon–oxygen cores and $M_{\rm H}/M* = 10^{-4}$ were used.

4.1 Synthetic fluxes

In the course of fitting procedure, we calculate synthetic fluxes for both BS and WD in GALEX and SDSSS bandpasses. The synthetic spectra can be converted to a monochromatic flux for a given bandpass via

$$f = \frac{\int_{\lambda_i}^{\lambda_f} \lambda f_\lambda S_\lambda {\rm d}\lambda}{\int_{\lambda_i}^{\lambda_f} \lambda S_\lambda {\rm d}\lambda} \quad (3)$$

where f_λ is the flux at a given wavelength λ and S_λ is the filter response at a given wavelength. The integration limits are the minimum and maximum wavelength of the bandpass.

4.2 Observed fluxes

The observed, extinction corrected, magnitudes were transformed to fluxes using the standard formulas. For SDSS bandpasses (Fukugita et al. 1996),

$$m_{\rm AB} = -2.5 \log f_\nu - 48.6 \quad (4)$$

The FUV and NUV fluxes are determined by means of the conversion,

$$m_{\rm FUV} = -2.5 \log \frac{{\rm Flux_{FUV}}}{1.40 * 10^{-15}} + 18.82 \quad (5)$$

$$m_{\rm NUV} = -2.5 \log \frac{{\rm Flux_{NUV}}}{2.06 * 10^{-16}} + 20.08 \quad (6)$$

[2]Kurucz models are available at http:kurucz.harvard.edu
[3]http://www.as.utexas.edu/ hebe/

4.3 SED fitting

In the fitting process we minimize the following chi-square function:

$$\chi^2 = \sum_i \frac{(\alpha^2 f_{\mathrm{wd},i} + \beta^2 f_{\mathrm{bs},i} - F_i)^2}{\sigma_{F,i}^2}, \tag{7}$$

where i is sum over all bandpasses.

$f_{\mathrm{bs},\,i}, f_{\mathrm{wd},\,i}, F_i$ are the flux of the BS model, flux of the WD model, and flux of the observed star, respectively. $\alpha = (R_{\mathrm{bs}}/D)$ and $\beta = (R_{\mathrm{wd}}/D)$ are scale factors and depend on radii (R_{bs} and R_{wd}) of each component and the distance (D).

The radii of both components (R_{bs}, R_{wd}) and distance are necessary as scale factors for the individual fluxes when combining the atmosphere models of both components to a single SED. However, for WD models the mass and the surface gravity are known. So for each model in the grid we can calculate the radius, according to

$$R_{\mathrm{WD}} = \sqrt{\frac{G M_{\mathrm{WD}}}{g_{\mathrm{WD}}}} \tag{8}$$

For the BS, we first obtain absolute magnitude calibration for our sample. We used transformation equations given by Zhao & Newberg (2006), which were derived from the SDSS stars with known UBVRI photometry, including a sample of BSS stars.

$$V = g - 0.561(g - r) - 0.004 \tag{9}$$

$$(B - V) = 0.916(g - r) + 0.187 \tag{10}$$

These transformations are valid within the range $-0.5 < g - r < 1.0$ (Beers et al. 2012), which is consistent with the color range we adopted here.

Using the V magnitude we obtained from equation (9), we can now calculate the absolute magnitude in V band (M_v) using the relation given by Kinman et al. (1994):

$$M_v = 1.32 + 4.05(B - V) - 0.45 \left[\frac{\mathrm{Fe}}{\mathrm{H}}\right]. \tag{11}$$

This relation was constructed by studying the BSs in globular clusters with different metallicities covering a wide range of colors and absolute magnitudes.

The luminosity of the star can be found by the use of M_v and bolometric correction in equation (12).

$$\left(\frac{L}{L_o}\right) = 10^{-0.4[M_v - V_o - 31.752 + (BC_v - BC_{v,o})]} \tag{12}$$

where we adopt the bolometric corrections given by Torres (2010).

Then, the radius of the BS can be estimated by the use of the relation,

$$\left(\frac{R}{R_o}\right) = \left(\frac{T_o}{T_{\mathrm{eff}}}\right)^2 \left(\frac{L}{L_o}\right)^{0.5} \tag{13}$$

To select the best-fitting white dwarf model, the χ^2 value of each fit is calculated by using equation (7). The optimal SED fits for four stars are shown in the top panel of Fig. 2. The presence of a hot white dwarf companion in a BS binary causes the excess FUV emission of the system. This is clear in Fig. 2. The expected emission from BSs without WD companions is much fainter than the observed flux at FUV. Adding WD companions of increasing temperature results in bright, blue emission as evidence by the best-fitting composite model (see black line in Fig. 2: top panel).

4.4 WD parameters

The distributions of mass, age, and effective temperatures of the white dwarfs determined from our SED fitting routine are shown in the bottom panel of Fig. 2. The most striking features of the distributions are as follows: vast majority of white dwarfs are very young (few million years old) and with temperatures range between 20 000 and 40 000K (see the bottom panel of Fig. 2). This is consistent with our initial selection criteria of BS, as recently formed BS are expected to have much larger UV excess. One interesting feature of the mass distribution is the peak at white dwarf mass 0.43 $\mathrm{M}_\odot$. White dwarf stars with masses below 0.47 $\mathrm{M}_\odot$ are thought to be He-core white dwarfs. (Core helium ignition starts when the core mass is roughly 0.47$\mathrm{M}_\odot$.) At the stage when mass transfer occurs, the expanding red giant core has not yet fully grown, therefore the resultant white dwarf will have a lower mass. If these WDs were single stars, they would have main sequence life times greater than age of the Universe. Therefore, these systems must be products of case B mass transfer, the only possible solution for producing such low-mass white dwarfs.

On the other hand, white dwarfs with masses > 0.5 $\mathrm{M}_\odot$ are consistent with predictions from case C, i.e. mass transfer from an asymptotic giant to a main sequence star that produces a carbon–oxygen white dwarf companion with mass of $\sim$0.5$\mathrm{M}_\odot$ to 0.6 $\mathrm{M}_\odot$ dictated by the core mass of the asymptotic giant donor at the end of the mass transfer phase (Hurley et al. 2002). The WD mass distribution in the Galactic field peaks at about 0.59 $\mathrm{M}_\odot$ and exhibits a significant low-mass tail of white dwarfs with masses lower than 0.45 $\mathrm{M}_\odot$, which peaks at 0.40 $\mathrm{M}_\odot$. These white dwarfs are predominantly found in close binary systems, mostly with another white dwarf or a neutron star companion (Momany et al. 2004). Interestingly, the low-mass end of this distribution is consistent with our results as well.

4.5 Mass transfer efficiency

Mass transfer efficiency β is defined as the mass fraction of the lost mass from the primary accreted by the secondary. This is an important parameter for binary evolution calculations where β is frequently treated with a constant value due to its large uncertainty (De Greve & De Loore 1992; Chen & Han 2009). Lu et al. (2010) used Monte Carlo simulations to investigate the origin of BS population in M67. In their calculations they used the $\beta = 0.5$ and $\beta = 1.0$ (fully conservative mass transfer, i.e. no mass or angular momentum loss from the system) and found that the higher value could reproduce the data better. Our WD parameters obtained via the BS-WD fitting can be used to infer a lower limit for β in our current sample.

The amount of mass transferred from the now WD to BS, δM_t,

$$\delta M_{\mathrm{trans}} = M_i - M_{\mathrm{wd}} \tag{14}$$

where M_i is the progenitor mass of the WD.

We interpolate theoretical relations that were constructed using BaSTI evolutionary models (Pietrinferni et al. 2006) so that we can calculate the progenitor mass at a given metallicity and age. We adopted the non-canonical BaSTI models with the mass loss efficiency of the Reimers law (Reimers 1977) set to $\eta = 0.2$. The initial He mass fraction ranges from 0.245 to 0.303, for the more metal-poor to the more metal-rich composition, respectively.

Jofré & Weiss (2011) estimated the ages of field halo stars using a sample of SDSS stars. They estimated a mean age 11 Gyr, which we adopted in our calculations to determine the mass from interpolated

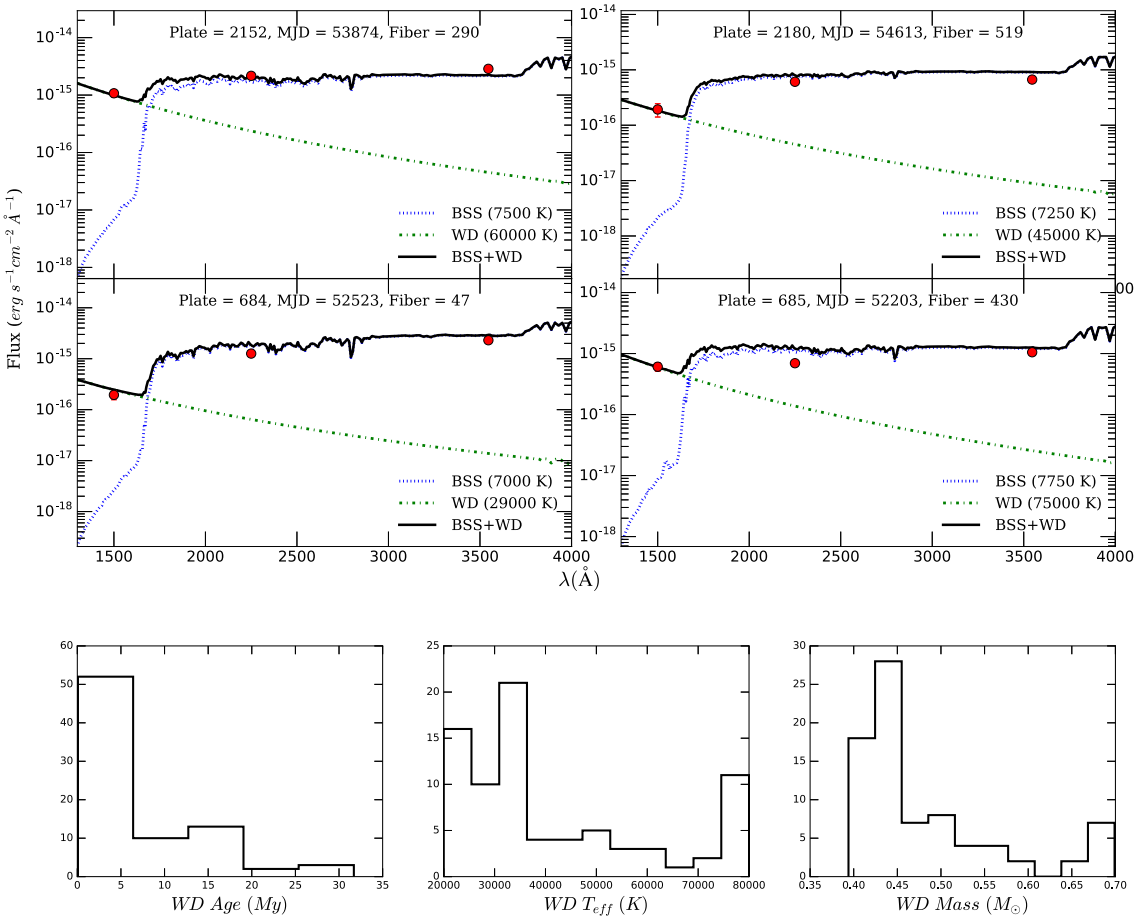

Figure 2. Top panel: Examples of BS+WD fitting. Red circles are the observed FUV, NUV, and *u* band fluxes. Blue and green dashed lines represent the synthetic spectra of BS and WD, respectively. Black solid line is the composite (BS+WD) best-fitting spectrum to the observed fluxes. Bottom panel: White Dwarf parameter distributions obtained from SED fitting.

BASTI models. The field stars of Jofré & Weiss (2011) have a mean metallicity of −1.7 dex. To be consistent with that work, we limited our sample to the stars with [Fe/H] < -1.35. This reduces our sample to 35 stars.

To calculate the amount of mass transferred, the initial mass of the secondary star (now the BS) is required. This initial mass value cannot be readily inferred, without first knowing the value of β. But we can estimate the lower limit of the transferred mass by considering the halo turnoff mass of 0.8 $M_\odot$, Then the mass accreted on to the secondary (now BS) is given by

$$\delta M_{\rm acc} = M_{\rm BS} - 0.8 \qquad (15)$$

Ratio of equations (15) and (14) will give the lower limit of the mass transfer efficiency. The derived β values are shown as a histogram in Fig. 3. All the stars have mass transfer efficiencies above $\beta \sim 0.5$. The value we obtained for the lower limit of β provides clues about the nature of these ancient, low-mass binary systems. The tendency for our systems to favor a more conservative mass tranfer (larger β) should help to inform tranfer models where donor initial mass is less than 1.0 $M_\odot$.

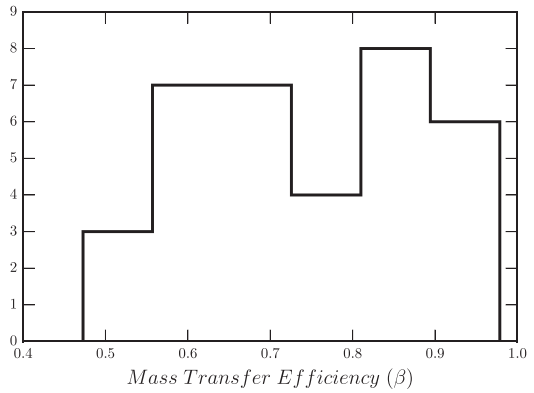

Figure 3. Histogram of the lower limits of the mass transfer efficiencies.

5 SUMMARY

We utilized UV-optical SED study of the BS binaries in the Galactic field. Using our fitting routine, we identified WD companions of field BSs formed by mass transfer. We found that these BSs have significant FUV excess by comparing the observed SED to a composite model with WD and BS components.

We found that our sample WDs range in age from a few million to a few tens of millions of years, suggesting that mass transfer in these binaries ended relatively recently. In addition, we conclude that the majority of the WD companions are helium WDs. Mass transfer from RGB stars in binary systems is the obvious way to produce such low-mass stars.

Combining the WD stellar parameters with the evolutionary models, we estimated the lower limit of the binary mass transfer efficiency in these stars to be, $\beta = 0.5$.

In order to determine the exact formation mechanisms for a particular population of BSs, a detailed characterization of the BSs is needed. This requires determining the rotation velocities and binary orbital parameters. Since the formation channel for BS binaries can distinguish from the type of companion star expected, it is vital to identify the observational constraints of the companion. These binaries will be good test cases for binary mass transfer modeling efforts in the future.

ACKNOWLEDGEMENTS

The authors would like to thank our referee, George Preston, for his insightful comments and suggestions that improved the overall content and flow of this paper.

This work made use of the public data services provided by MAST, SDSS and CDS.

REFERENCES

Beers T. C. et al., 2012, ApJ, 746, 34
Castelli F., Kurucz R. L., 2014, preprint (arXiv: astro-ph/0405087)
Chen X., Han Z., 2009, MNRAS, 395, 1822
De Greve J. P., De Loore C., 1992, A&AS, 96, 653
Deng L., Chen R., Liu X. S., Chen J. S., 1999, ApJ, 524, 824
Ferraro F. R. , Paltrinieri B. , Rood R. T., Dorman B., 1999, ApJ, 522, 983
Fontaine G., Brassard P., Bergeron P. et al., 2001, PASP, 113, 409
Fukugita M., Ichikawa T., Gunn J. E., Doi M., Shimasaku K., Schneider D. P., 1996, AJ, 111, 1748
Gosnell N. M., Mathieu R. D., Geller A. M., Sills A., Leigh N., Knigge C., 2014, ApJ, 783, L8
Gray R. O., Corbally C. J., 1994, AJ, 107, 742
Hurley J. R., Tout C. A., Pols O. R., 2002, MNRAS, 329, 897
Jofré P., Weiss A., 2011, A&A, 533, A59
Kinman T. D., Suntzeff N. B., Kraft R. P., 1994, AJ, 108, 1722
Kippenhahn R., Weigert A., 1967, ZAp, 65, 251
Lee Y. S. et al., 2008, AJ, 136, 2022
Lu P., Deng L. C., Zhang X. B., 2010, MNRAS, 409, 1013
McCrea W. H., 1964, MNRAS, 128, 147
Momany Y., Held E. V., Saviane I., Zaggia S., Rizzi L., Gullieuszik M., 2007, A&A, 468, 973
Momany Y., Zaggia S. R. , Bonifacio P., Piotto G., De Angeli F., Bedin L. R., Carraro G., 2004, A&A, 421, L29
Pietrinferni A., Cassisi S., Salaris M., Castelli F., 2006, ApJ, 642, 797
Preston G. W., Preston A. U., 1999, AJ, 118, 3006
Preston G. W., Sneden C., 2000, AJ, 120, 1014
Rebassa-Mansergas A., Nebot Gomez-Moran A., Schreiber M. R., Gansicke B. T., Schwope A., Gallardo J., Koester D., 2012, MNRAS, 419, 806
Rey S.-C. et al., 2007, ApJS, 173, 643
Ryan S. G., Gregory S. G., Kolb U., Beers T., Kajino T., 2002, ApJ, 571, 501
Sandage A. R., AJ, 1953, 58, 61
Mathieu R. D., Geller A. M., 2009, Nature, 462, 1032
Schlafly E. F., Finkbeiner D. P., 2011, ApJ, 737, 103
Schlegel D. J., Finkbeiner D. P., Davis M., 1998, ApJ, 500, 525
Sirko E. et al., 2004, AJ, 127, 914
Smith M. A. , et al., 2014, AJ, 147, 159
Tamás B. et al., 2009, ApJ, 694, 1281
Torres G., 2010, AJ, 140, 1158
Wood M. A., 1995, Theoretical White Dwarf Luminosity Functions: DA Models. Vol. 443 of Lecture Notes in Physics, Springer Verlag, Berlin, p. 41
Xue X. X. et al., 2008, ApJ, 684, 1143
Yanny B. et al., 2000, ApJ, 540, 825
Zhao, Newberg H. J., 2006, preprint (arXiv:astro-ph/0612034)

APPENDIX A:

Table A1. Stellar parameters and photometry of UV-excess BSs.

SDSS ID	$T_{\rm eff}$	log g	[*Fe*/*H*]	FUV	NUV	*u*	*g*	*r*	*i*	*z*
915-52443-549	7423 ± 157	3.84 ± 0.49	− 0.69 ± 0.2	19.0 ± 0.17	17.13 ± 0.04	15.76 ± 0.02	14.71 ± 0.01	14.68 ± 0.02	14.73 ± 0.01	14.82 ± 0.02
740-52263-440	7673 ± 129	4.32 ± 0.15	− 1.98 ± 0.07	19.89 ± 0.24	19.35 ± 0.13	18.64 ± 0.02	17.84 ± 0.01	17.89 ± 0.01	17.94 ± 0.02	18.07 ± 0.03
684-52523-47	7004 ± 40	3.88 ± 0.23	− 0.78 ± 0.05	20.93 ± 0.21	18.06 ± 0.03	16.41 ± 0.03	15.44 ± 0.02	15.3 ± 0.01	15.27 ± 0.02	15.34 ± 0.02
3131-54731-429	7936 ± 110	4.36 ± 0.03	− 1.35 ± 0.1	20.08 ± 0.25	19.57 ± 0.07	18.55 ± 0.03	17.53 ± 0.02	17.56 ± 0.01	17.62 ± 0.01	17.59 ± 0.03
2951-54592-114	7615 ± 73	3.93 ± 0.44	− 2.07 ± 0.16	19.42 ± 0.24	18.64 ± 0.1	17.55 ± 0.02	16.51 ± 0.02	16.49 ± 0.01	16.54 ± 0.01	16.57 ± 0.02
2849-54454-349	7083 ± 37	4.21 ± 0.29	− 1.53 ± 0.02	19.46 ± 0.18	17.57 ± 0.05	16.22 ± 0.01	15.32 ± 0.02	15.2 ± 0.02	15.16 ± 0.01	15.22 ± 0.02
1894-53240-211	7441 ± 78	4.19 ± 0.21	− 1.25 ± 0.08	21.18 ± 0.26	19.58 ± 0.04	18.48 ± 0.02	17.44 ± 0.02	17.33 ± 0.01	17.37 ± 0.01	17.43 ± 0.02
2299-53711-626	7742 ± 64	3.93 ± 0.18	− 0.25 ± 0.04	21.67 ± 0.43	20.53 ± 0.19	18.71 ± 0.03	17.61 ± 0.01	17.61 ± 0.01	17.7 ± 0.02	17.81 ± 0.03
2299-53711-453	7460 ± 50	3.88 ± 0.21	− 0.24 ± 0.08	21.01 ± 0.48	19.53 ± 0.16	17.69 ± 0.02	16.5 ± 0.01	16.45 ± 0.01	16.5 ± 0.01	16.58 ± 0.01
2848-54453-473	7032 ± 31	4.14 ± 0.25	− 1.41 ± 0.04	19.47 ± 0.1	17.15 ± 0.02	15.9 ± 0.01	14.95 ± 0.02	14.82 ± 0.02	14.81 ± 0.02	14.88 ± 0.01
1254-52972-515	7672 ± 140	4.2 ± 0.11	− 0.02 ± 0.05	18.66 ± 0.38	17.5 ± 0.12	15.96 ± 0.02	15.01 ± 0.01	15.07 ± 0.02	15.15 ± 0.01	15.33 ± 0.01
1252-52970-306	7791 ± 0	4.14 ± 0.23	− 0.25 ± 0.03	16.95 ± 0.11	16.75 ± 0.06	16.28 ± 0.02	15.4 ± 0.02	15.41 ± 0.01	15.48 ± 0.01	15.61 ± 0.02
2335-53730-480	7468 ± 33	3.98 ± 0.31	− 0.49 ± 0.14	19.14 ± 0.46	17.75 ± 0.15	16.04 ± 0.05	14.98 ± 0.02	14.9 ± 0.02	14.97 ± 0.02	15.02 ± 0.02
3241-54884-335	8029 ± 71	4.13 ± 0.2	− 1.97 ± 0.25	19.3 ± 0.21	18.9 ± 0.13	18.16 ± 0.04	17.23 ± 0.02	17.32 ± 0.01	17.42 ± 0.01	17.54 ± 0.02
685-52203-430	7686 ± 112	3.93 ± 0.36	− 1.03 ± 0.07	19.69 ± 0.17	18.7 ± 0.08	17.26 ± 0.01	16.11 ± 0.02	16.09 ± 0.02	16.12 ± 0.02	16.15 ± 0.02
3130-54740-107	7344 ± 69	4.15 ± 0.22	− 1.89 ± 0.07	19.87 ± 0.19	19.32 ± 0.07	18.45 ± 0.02	17.45 ± 0.02	17.38 ± 0.01	17.35 ± 0.02	17.43 ± 0.02
2252-53565-281	7301 ± 44	4.19 ± 0.16	− 0.27 ± 0.04	21.02 ± 0.39	19.05 ± 0.05	17.4 ± 0.01	16.32 ± 0.02	16.24 ± 0.01	16.26 ± 0.01	16.3 ± 0.01
1961-53299-168	7291 ± 45	4.05 ± 0.19	− 0.76 ± 0.02	19.49 ± 0.17	18.25 ± 0.07	17.61 ± 0.02	16.61 ± 0.01	16.53 ± 0.02	16.54 ± 0.02	16.62 ± 0.02
1960-53289-343	7127 ± 33	4.23 ± 0.17	− 0.54 ± 0.06	20.9 ± 0.4	18.45 ± 0.09	16.71 ± 0.02	15.68 ± 0.02	15.54 ± 0.01	15.54 ± 0.02	15.57 ± 0.02
3138-54740-521	7381 ± 31	4.03 ± 0.3	− 1.11 ± 0.03	21.04 ± 0.45	19.95 ± 0.19	18.44 ± 0.03	17.4 ± 0.01	17.31 ± 0.01	17.35 ± 0.02	17.38 ± 0.02
3138-54740-401	7562 ± 177	4.31 ± 0.16	− 2.59 ± 0.01	19.49 ± 0.21	19.08 ± 0.12	17.77 ± 0.03	16.76 ± 0.01	16.75 ± 0.01	16.73 ± 0.01	16.71 ± 0.02
1857-53182-27	7343 ± 129	4.31 ± 0.2	− 0.88 ± 0.08	21.53 ± 0.34	20.45 ± 0.19	18.87 ± 0.03	17.9 ± 0.01	17.77 ± 0.01	17.79 ± 0.01	17.88 ± 0.03
366-52017-28	7320 ± 60	4.2 ± 0.23	− 1.01 ± 0.08	21.16 ± 0.37	19.37 ± 0.12	17.88 ± 0.02	16.91 ± 0.02	16.86 ± 0.01	16.86 ± 0.02	16.92 ± 0.02
2797-54616-614	8005 ± 47	4.24 ± 0.19	− 1.22 ± 0.32	20.87 ± 0.38	20.41 ± 0.26	18.74 ± 0.04	17.67 ± 0.01	17.71 ± 0.01	17.81 ± 0.02	17.92 ± 0.03
2551-54552-257	7368 ± 100	4.07 ± 0.06	− 1.31 ± 0.06	21.51 ± 0.34	19.91 ± 0.12	18.75 ± 0.02	17.58 ± 0.02	17.51 ± 0.02	17.52 ± 0.02	17.52 ± 0.03
2247-53857-96	7290 ± 68	4.18 ± 0.29	− 0.54 ± 0.04	20.57 ± 0.34	19.57 ± 0.14	18.18 ± 0.02	17.1 ± 0.02	17.05 ± 0.01	17.08 ± 0.01	17.15 ± 0.02
2180-54613-519	7368 ± 46	3.98 ± 0.31	− 1.83 ± 0.01	20.94 ± 0.29	18.85 ± 0.06	17.75 ± 0.02	16.89 ± 0.02	16.87 ± 0.02	16.87 ± 0.02	16.92 ± 0.02
1659-53224-452	7530 ± 40	4.05 ± 0.19	− 0.56 ± 0.09	19.56 ± 0.15	17.9 ± 0.05	16.46 ± 0.02	15.39 ± 0.01	15.38 ± 0.01	15.45 ± 0.02	15.55 ± 0.02
2550-54206-232	7097 ± 80	4.24 ± 0.14	− 0.97 ± 0.05	21.17 ± 0.36	18.61 ± 0.07	17.16 ± 0.02	16.15 ± 0.01	16.04 ± 0.02	16.02 ± 0.02	16.04 ± 0.02
2189-54624-640	7307 ± 61	4.0 ± 0.67	− 1.5 ± 0.0	21.51 ± 0.45	19.91 ± 0.11	18.71 ± 0.03	17.74 ± 0.02	17.73 ± 0.01	17.75 ± 0.01	17.84 ± 0.03
595-52023-92	7542 ± 81	4.11 ± 0.08	− 1.72 ± 0.04	19.07 ± 0.18	17.99 ± 0.05	16.88 ± 0.02	15.89 ± 0.01	15.87 ± 0.01	15.92 ± 0.01	15.98 ± 0.02
1727-53859-288	7045 ± 39	3.84 ± 0.43	− 0.53 ± 0.02	21.79 ± 0.43	20.25 ± 0.14	18.61 ± 0.02	17.52 ± 0.02	17.42 ± 0.02	17.42 ± 0.02	17.48 ± 0.02
2782-54592-113	7445 ± 103	3.88 ± 0.45	− 1.61 ± 0.05	19.64 ± 0.21	19.26 ± 0.12	18.33 ± 0.02	17.23 ± 0.01	17.16 ± 0.01	17.12 ± 0.01	17.11 ± 0.02
3308-54919-447	7368 ± 82	3.92 ± 0.4	− 1.41 ± 0.09	20.9 ± 0.37	19.81 ± 0.14	18.8 ± 0.03	17.95 ± 0.02	17.91 ± 0.01	17.96 ± 0.02	18.04 ± 0.03
2781-54266-417	7768 ± 145	4.37 ± 0.16	− 1.34 ± 0.03	20.35 ± 0.26	19.28 ± 0.11	18.16 ± 0.02	17.23 ± 0.02	17.31 ± 0.01	17.34 ± 0.01	17.41 ± 0.02
2156-54525-520	7483 ± 58	3.89 ± 0.42	− 0.98 ± 0.02	21.75 ± 0.42	20.26 ± 0.14	18.71 ± 0.02	17.7 ± 0.01	17.68 ± 0.02	17.74 ± 0.01	17.83 ± 0.02
3297-54941-411	7411 ± 56	3.98 ± 0.45	− 1.14 ± 0.17	19.99 ± 0.28	18.52 ± 0.08	17.34 ± 0.02	16.33 ± 0.02	16.27 ± 0.02	16.3 ± 0.02	16.32 ± 0.02
2152-53874-290	7557 ± 40	4.14 ± 0.23	− 1.02 ± 0.09	19.07 ± 0.16	17.47 ± 0.05	16.17 ± 0.01	15.11 ± 0.02	15.11 ± 0.01	15.17 ± 0.01	15.26 ± 0.02
3406-54970-104	7191 ± 81	4.32 ± 0.02	− 1.98 ± 0.02	21.27 ± 0.32	19.92 ± 0.11	18.77 ± 0.02	17.87 ± 0.02	17.79 ± 0.02	17.77 ± 0.03	17.83 ± 0.02
3406-54970-518	7335 ± 50	4.25 ± 0.18	− 1.79 ± 0.04	21.91 ± 0.44	19.89 ± 0.11	18.8 ± 0.02	17.9 ± 0.02	17.8 ± 0.01	17.82 ± 0.01	17.86 ± 0.03
3387-54951-106	7979 ± 116	4.21 ± 0.38	− 1.84 ± 0.21	20.53 ± 0.4	20.07 ± 0.2	18.75 ± 0.02	17.73 ± 0.02	17.73 ± 0.02	17.87 ± 0.02	17.99 ± 0.02
3384-54948-315	7403 ± 67	3.89 ± 0.33	− 1.92 ± 0.07	21.29 ± 0.28	19.45 ± 0.07	18.29 ± 0.02	17.3 ± 0.02	17.24 ± 0.02	17.25 ± 0.02	17.32 ± 0.02
1348-53084-179	7652 ± 15	4.19 ± 0.21	− 2.24 ± 0.0	19.6 ± 0.18	18.53 ± 0.06	17.59 ± 0.02	16.59 ± 0.01	16.59 ± 0.02	16.67 ± 0.02	16.69 ± 0.02
2124-53770-535	7005 ± 44	4.08 ± 0.04	− 1.45 ± 0.05	21.25 ± 0.45	18.57 ± 0.09	17.13 ± 0.02	16.25 ± 0.01	16.12 ± 0.01	16.12 ± 0.01	16.15 ± 0.01
2336-53712-115	7469 ± 22	4.07 ± 0.23	− 0.6 ± 0.07	21.01 ± 0.4	19.96 ± 0.19	18.5 ± 0.02	17.46 ± 0.02	17.4 ± 0.01	17.45 ± 0.01	17.52 ± 0.02
424-51893-60	7176 ± 23	3.93 ± 0.11	− 0.61 ± 0.09	21.31 ± 0.46	18.84 ± 0.09	17.09 ± 0.02	16.04 ± 0.02	15.94 ± 0.02	15.95 ± 0.01	16.0 ± 0.02
2445-54573-173	7317 ± 87	4.25 ± 0.34	− 1.37 ± 0.46	21.78 ± 0.34	19.85 ± 0.1	18.72 ± 0.02	17.66 ± 0.02	17.57 ± 0.02	17.65 ± 0.02	17.69 ± 0.02
1282-52759-79	7541 ± 52	3.83 ± 0.35	− 1.8 ± 0.13	21.1 ± 0.37	19.53 ± 0.11	18.32 ± 0.02	17.22 ± 0.03	17.23 ± 0.01	17.29 ± 0.01	17.36 ± 0.02
3377-54950-189	7349 ± 31	4.13 ± 0.35	− 1.38 ± 0.09	19.95 ± 0.21	18.83 ± 0.07	17.75 ± 0.02	16.84 ± 0.01	16.78 ± 0.01	16.81 ± 0.02	16.84 ± 0.02
2899-54568-252	7164 ± 29	4.01 ± 0.12	− 0.22 ± 0.05	20.04 ± 0.23	17.51 ± 0.04	15.63 ± 0.03	14.57 ± 0.02	14.46 ± 0.02	14.47 ± 0.01	14.56 ± 0.02
1456-53115-620	7072 ± 59	3.9 ± 0.27	− 0.84 ± 0.04	21.53 ± 0.48	18.97 ± 0.05	17.32 ± 0.02	16.22 ± 0.02	16.14 ± 0.02	16.18 ± 0.02	16.24 ± 0.02
2661-54505-400	7402 ± 59	4.13 ± 0.12	− 0.7 ± 0.08	20.64 ± 0.27	18.93 ± 0.05	17.65 ± 0.02	16.61 ± 0.02	16.59 ± 0.01	16.62 ± 0.01	16.71 ± 0.01
335-52000-452	7758 ± 159	4.1 ± 0.16	− 2.03 ± 0.06	19.58 ± 0.19	19.11 ± 0.1	18.49 ± 0.02	17.54 ± 0.02	17.61 ± 0.01	17.66 ± 0.01	17.7 ± 0.02
2647-54495-235	7096 ± 51	3.9 ± 0.12	− 1.47 ± 0.02	21.61 ± 0.42	19.04 ± 0.09	17.62 ± 0.02	16.66 ± 0.02	16.56 ± 0.02	16.55 ± 0.02	16.59 ± 0.02
3253-54941-210	7296 ± 41	3.96 ± 0.27	− 1.74 ± 0.04	21.47 ± 0.47	19.29 ± 0.07	17.99 ± 0.02	17.06 ± 0.02	17.0 ± 0.02	17.03 ± 0.02	17.08 ± 0.02
334-51993-267	7270 ± 74	3.94 ± 0.28	− 1.38 ± 0.01	21.78 ± 0.41	20.32 ± 0.13	18.76 ± 0.02	17.7 ± 0.02	17.63 ± 0.02	17.66 ± 0.01	17.71 ± 0.02
3214-54866-426	7159 ± 49	3.85 ± 0.3	− 1.68 ± 0.04	21.69 ± 0.48	19.99 ± 0.16	18.55 ± 0.04	17.6 ± 0.02	17.57 ± 0.02	17.55 ± 0.02	17.61 ± 0.02
2892-54552-128	7256 ± 80	3.84 ± 0.37	− 1.99 ± 0.13	22.22 ± 0.3	19.94 ± 0.08	18.67 ± 0.02	17.82 ± 0.02	17.71 ± 0.01	17.71 ± 0.01	17.77 ± 0.02
3285-54948-131	7509 ± 116	3.94 ± 0.2	− 1.66 ± 0.02	18.48 ± 0.1	17.79 ± 0.05	16.93 ± 0.03	15.98 ± 0.03	16.03 ± 0.03	16.06 ± 0.02	16.14 ± 0.03
2512-53877-326	7061 ± 48	3.86 ± 0.16	− 2.04 ± 0.09	21.44 ± 0.38	18.85 ± 0.04	17.48 ± 0.02	16.5 ± 0.01	16.41 ± 0.02	16.44 ± 0.01	16.46 ± 0.02
3170-54859-111	7520 ± 98	4.23 ± 0.31	− 2.39 ± 0.05	20.12 ± 0.14	18.93 ± 0.04	17.87 ± 0.02	16.86 ± 0.01	16.82 ± 0.01	16.84 ± 0.02	16.89 ± 0.02
878-52353-617	7240 ± 51	4.14 ± 0.31	− 1.81 ± 0.16	20.61 ± 0.3	18.79 ± 0.07	17.41 ± 0.02	16.44 ± 0.02	16.33 ± 0.02	16.36 ± 0.03	16.38 ± 0.02
3193-54830-593	7838 ± 78	4.19 ± 0.22	− 1.14 ± 0.02	20.44 ± 0.22	19.71 ± 0.11	18.66 ± 0.03	17.55 ± 0.02	17.62 ± 0.01	17.66 ± 0.02	17.75 ± 0.03
267-51608-422	7336 ± 59	3.98 ± 0.32	− 1.55 ± 0.06	21.55 ± 0.36	19.96 ± 0.1	18.5 ± 0.02	17.5 ± 0.02	17.44 ± 0.02	17.49 ± 0.02	17.56 ± 0.03
1739-53050-128	7533 ± 73	3.98 ± 0.16	− 2.23 ± 0.05	20.89 ± 0.37	19.31 ± 0.08	18.01 ± 0.02	16.98 ± 0.02	16.81 ± 0.01	16.87 ± 0.02	17.13 ± 0.02
1934-53357-4	7408 ± 39	4.03 ± 0.09	− 1.43 ± 0.15	21.64 ± 0.28	20.35 ± 0.12	19.02 ± 0.03	17.97 ± 0.03	17.95 ± 0.02	17.98 ± 0.02	18.02 ± 0.04
1590-52974-388	7126 ± 23	3.95 ± 0.05	− 0.24 ± 0.02	21.86 ± 0.46	19.31 ± 0.1	17.71 ± 0.02	16.58 ± 0.01	16.49 ± 0.02	16.51 ± 0.02	16.57 ± 0.02
3195-54832-552	7059 ± 34	4.07 ± 0.14	− 0.42 ± 0.03	20.81 ± 0.39	18.9 ± 0.1	17.32 ± 0.02	16.3 ± 0.02	16.22 ± 0.02	16.2 ± 0.01	16.26 ± 0.01
3230-54860-409	7081 ± 54	4.34 ± 0.14	− 0.42 ± 0.07	20.77 ± 0.37	18.49 ± 0.08	16.74 ± 0.02	15.65 ± 0.02	15.55 ± 0.02	15.58 ± 0.02	15.63 ± 0.02
2273-53709-207	7353 ± 128	4.05 ± 0.32	− 0.48 ± 0.13	20.97 ± 0.4	19.41 ± 0.12	18.1 ± 0.02	16.86 ± 0.02	16.72 ± 0.01	16.67 ± 0.01	16.62 ± 0.01
3230-54860-353	7541 ± 69	3.89 ± 0.27	− 1.52 ± 0.05	21.47 ± 0.49	19.89 ± 0.17	18.76 ± 0.02	17.75 ± 0.01	17.71 ± 0.02	17.77 ± 0.02	17.84 ± 0.02
3226-54857-452	8004 ± 116	4.15 ± 0.17	− 0.52 ± 0.17	18.15 ± 0.11	17.89 ± 0.02	17.58 ± 0.02	16.66 ± 0.01	16.74 ± 0.01	16.86 ± 0.01	16.99 ± 0.02
758-52253-5	7930 ± 117	3.99 ± 0.18	− 1.34 ± 0.04	18.47 ± 0.12	18.45 ± 0.04	18.45 ± 0.03	17.75 ± 0.02	17.79 ± 0.02	17.92 ± 0.01	18.05 ± 0.03
2420-54086-395	7780 ± 101	4.07 ± 0.38	− 1.47 ± 0.05	21.25 ± 0.35	20.17 ± 0.12	18.82 ± 0.02	17.84 ± 0.01	17.8 ± 0.01	17.87 ± 0.01	17.94 ± 0.02
2541-54481-384	7282 ± 26	3.87 ± 0.0	− 0.24 ± 0.01	20.22 ± 0.21	18.0 ± 0.04	16.32 ± 0.02	15.26 ± 0.01	15.16 ± 0.03	15.17 ± 0.02	15.25 ± 0.02
2055-53729-37	7297 ± 44	3.99 ± 0.25	− 0.56 ± 0.05	19.97 ± 0.17	17.86 ± 0.04	16.37 ± 0.01	15.32 ± 0.02	15.26 ± 0.0	15.27 ± 0.01	15.35 ± 0.01
3166-54830-409	7203 ± 14	4.18 ± 0.12	− 0.45 ± 0.03	20.72 ± 0.34	18.28 ± 0.07	16.59 ± 0.02	15.55 ± 0.01	15.46 ± 0.01	15.49 ± 0.02	15.61 ± 0.02
3161-54779-445	7351 ± 62	4.04 ± 0.23	− 0.81 ± 0.1	21.42 ± 0.48	19.45 ± 0.13	18.2 ± 0.02	17.13 ± 0.02	17.11 ± 0.01	17.22 ± 0.02	17.3 ± 0.02
2941-54507-638	7097 ± 25	4.09 ± 0.11	− 0.46 ± 0.02	20.89 ± 0.27	18.37 ± 0.04	16.64 ± 0.02	15.65 ± 0.01	15.51 ± 0.01	15.52 ± 0.01	15.57 ± 0.02
2337-53740-222	7100 ± 26	3.89 ± 0.17	− 0.24 ± 0.04	19.51 ± 0.17	17.98 ± 0.06	16.27 ± 0.01	15.17 ± 0.01	15.04 ± 0.01	15.04 ± 0.01	15.1 ± 0.01

This paper has been typeset from a TEX/LATEX file prepared by the author.